Research Article

Zahir Shah*, Muhammad Rooman, Naeem Ullah Khan, Muhammad Sulaiman, Mansoor H. Alshehri, Narcisa Vrinceanu*, and Mihaela Racheriu

Modeling and heat transfer analysis of magnetized hybrid micropolar blood-based nanofluid flow in Darcy–Forchheimer porous stenosis narrow arteries

https://doi.org/10.1515/phys-2025-0139
received November 17, 2024; accepted March 12, 2025

Abstract: This article provides a concise comparative examination of how heat generation affects the flow of a magnetized micropolar blood-based hybrid nanofluid (HNF) *via* a stenotic artery. The effects of Joule heating and viscous dissipation are considered. The purpose of this model is to evaluate and contrast the efficiency of HNF models. Our objective is to comprehend the complex process of hybridization by studying the behavior of titanium dioxide (TiO_2) and gold (Au) nanoparticles scattered in blood. The mathematical model has been converted into a dimensionless form by applying similarity transformations. This modified model is then efficiently solved using numerical methods, specifically bvp4c, which is a built-in command in MATLAB for solving boundary value problems, and facilitates the efficient handling of nonlinear ordinary differential equations with high accuracy and stability. The cylindrical surface is employed for the computation of flow measures, and the results are visually depicted using tables and graphs. This study makes a substantial contribution by uncovering previously unidentified flow characteristics. The use of Au nanoparticles demonstrates efficacy in improving the blood flow and offers a promising approach for addressing arterial disorders, as opposed to aluminum oxide nanoparticles. Moreover, an inquiry is carried out to examine the skin friction and heat transfer related to the dynamics of blood flow. The results demonstrate that the inclusion of Au and TiO_2 nanoparticles enhances heat transfer compared to single-component nanofluids (NFs) while effectively moderating the velocity and temperature profiles under varying conditions. Also, the HNF shows a reduction in temperature rise compared to NFs with only Au nanoparticles, under specific parameter settings.

Keywords: computational modeling, hybrid nanofluid, heat source, Darcy–Forchheimer, curved surface, stenotic artery, vicious and Joule dissipation, blood, gold nanoparticles

*** Corresponding author: Zahir Shah,** Department of Mathematical Sciences, University of Lakki Marwat, Lakki Marwat, 28420, Khyber Pakhtunkhwa, Pakistan, e-mail: Zahir@ulm.edu.pk
*** Corresponding author: Narcisa Vrinceanu,** Faculty of Engineering, Department of Industrial Machines and Equipments, "Lucian Blaga" University of Sibiu, 10 Victoriei Boulevard, Sibiu, Romania, e-mail: vrinceanu.narcisai@ulbsibiu.ro
Muhammad Rooman, Naeem Ullah Khan: Department of Mathematical Sciences, University of Lakki Marwat, Lakki Marwat, 28420, Khyber Pakhtunkhwa, Pakistan
Muhammad Sulaiman: Department of Mathematics, COMSATS Intitute of Information Technology, Attock, 43600, Pakistan
Mansoor H. Alshehri: Department of Mathematics, College of Science, King Saud University, P.O. Box 2455, Riyadh, 11451, Saudi Arabia
Mihaela Racheriu: Department of Clinical Surgery, Cty Clin Emergency Hosp, Sibiu, Romania

Nomenclature

B	micro-inertia density parameter (kg m^2)
Ec	Eckert number
F_r	coefficient of inertia
K	micropolar material parameter
M	magnetic parameter
N	microrotation (rad/s)
P	pressure (Pa)
Pr	Prandtl number
S	unsteady parameter
T	temperature (K)
V	velocity vector (m/s)
k_{f}	thermal conductivity (W/m K)
c_{p}	specific heat of nanoparticles (J/Kg K)

Greek

α, β, and γ	gyroviscosity coefficients

κ	vortex viscosity (Pa s)
u_f	dynamic viscosity (Pa s)
ρ_p	density of nanoparticles (kg/m^3)
σ_e	electrical conductivity (mS/m)

Subscript

h_{nf}	hybrid nanofluid
f	base fluid

1 Introduction

Micropolar fluids possess distinct microscopic properties and are characterized by the manifestation of rigid, spherical, or erratically oriented particles. When the microparticles are suspended in a thick liquid, they display distinct spins and little rotations. These are a class of polar fluids that possess a wide range of microscale activities, which are observed in a range of phenomena physically, such as blood circulation, liquid crystals, and bubbling liquids. As a result, this topic has gained significant recognition in the literature. Xu and Pop [1] have established a connection between advancements in nanofluids (NFs) and bioconvection through their latest study on micropolar fluids. Aziz *et al.* [2] proposed a theoretical model for the flow of an NF at the bio-convection boundary layer. Agarwal *et al.* [3] employed the finite element method to investigate the flow and heat transmission of a micropolar fluid over a stretching sheet. Hassanien and Gorla [4] studied the steady flow of boundary layers formed by permeable and impermeable sheets with micropolar movement. Rehman *et al.* [5] analyzed the stability influenced by shape factors in radiative magneto-hydrodynamic couple stress hybrid nanofluids (HNFs), and this work highlights how shape factors affect the stability of thermal and flow fields in complex fluids, with potential applications in industrial fluid systems.

The study conducted by Nadeem *et al.* [6] focused on examining the axisymmetric stagnation flow of a micropolar NF within a rotating cylinder. Balaram and Sastri [7] studied the natural flow of a micropolar fluid in a vertical tube with parallel plates. Lok *et al.* [8] constructed a continuous flow of data in two dimensions.

An HNF is a novel fusion of two or more dispersed nanoparticles in a base fluid. The objective of discovering HNFs is to optimize the heat transmission, enhance the thermal conductivity, and achieve stability by successfully merging the benefits and drawbacks of distinct suspensions. This is accomplished by the combined impact of nanomaterials, carefully adjusted proportions, an exceptional thermal network, and extensive utilization in diverse nuclear power-related domains, including generator cooling, machinery coolant, electronic cooling, and general cooling applications. The enhanced thermal conductivity exhibited by HNFs offers an opportunity to consider their potential application in addressing real-world thermal energy challenges. In their investigation, Waini *et al.* [9] investigated the effects of a hybrid nano-liquid on a surface that is both moving and permeable. The liquid included a constant volume portion for alumina nanoparticles and varying volume fraction for copper (Cu) nanoparticles. Ashwinkumar *et al.* [10] used non-linear thermal radiation to investigate the flow of an HNF consisting of $CuO–Al_2O_3$ in water. They specifically examined the parameters of the HNF flow past a vertical plate and a cone. Samrat and his team [11] investigated the impact of a stretched surface on heat transfer in the flow of dusty NF and HNF. Acharya [12] developed a simulation using spectral quasi-linearization to study the hydrothermal properties of HNFs when applied to a tilted spinning disc, and Sarwar and Hussain [13] worked on flow characteristics of the Au–blood NF in stenotic arteries. The results suggest that both the rotational speed of the disc and the proportion of nanoparticles in the volume have a significant influence on temperature distributions. Garia *et al.* [14] investigated the flow of HNFs on two different shapes. A mathematical correlation was constructed to quantify the magnitude of skin friction and the Nusselt number. The micro-polar liquid theory is a theoretical framework that considers the rotation of nanoparticles within a boundary layer. The studies of Eringen, Shah *et al.*, and Deebani *et al.* [15–17] suggest that micropolar fluids can be regarded as an enhancement of the Navier–Stokes condition. These systems are considered a subset of microfluidics due to consideration of the microstructure and the inertial characteristics of the particles inside the fluid that enable the experiment. In their study, Hassanien and Gorla [18] examined the heat transportation process from a stretching sheet to a micropolar fluid. The time-dependent flow of micropolar magnetohydrodynamic (MHD) fluid in a penetrable medium on a two-dimensional plane was examined by Subhani and Nadeem [19]. Hasegan *et al.* [20–22] investigated the blood flow and medical applications. MHD fluid refers to a fluid that experiences the influence of magnetic and electromagnetic forces. Some applications that utilize MHD are solar panels, polymer synthesis, and efficient boilers. A comprehensive study was carried out in this area to examine the manipulation of NFs using

electromagnetic forces, due to their considerable importance. Ghadikolaei *et al.* [23] investigated the manipulation of microliquid flow in a medium using magnetic field effects. The study conducted by Ullah *et al.* [24] investigated the impact of Newtonian heating and slip conditions on the MHD flow of a Casson fluid across a nonlinearly stretching sheet that is saturated in a porous medium. The study conducted by Gul *et al.* [25] investigated the heat transport in a fluid flow of ferrofluids with MHD mixed convection on a vertical passage. Saqib *et al.* [26] conducted a study on the natural convection channel flow of the CMC-based CNT NF. The results suggest that greater enhancement in heat transmission is achieved when lower volume fractions are used, matching the base fluid. Augmentation of the proportion of volume was demonstrated to lead to an elevation in the localized Nusselt number. A numerical examination of the MHD convection in NFs within a baffled U-shaped region was conducted by Ma *et al.* [27], whereas Khan *et al.* [28] studied how various models of nanoparticles influence the properties of peristaltic flow in MHD NFs in an irregular passage. Ghalambaz *et al.* [29] examined the presence of unstructured convection in an enclosed region containing a mix of nanoparticles of copper and aluminum oxide, recognized as Cu–Al_2O_3 HNFs. Zeb *et al.* [30] investigated the melting heat transfer and thermal radiation effects on MHD tangent hyperbolic NF flow, incorporating chemical reactions and activation energy. Das *et al.* [31] examined the production of entropy in the motion of Cu–Al_2O_3 HNFs in a porous channel under the effect of MHD. The findings indicate that when the volume fraction of nanoparticles increases, the production of entropy is reduced. The impact of viscous dissipation on the flow of micropolar fluids over a small stretching surface was explored by Anantha Kumar *et al.* [32], and they observed that as the value of micropolar parameters and viscous dissipation increase, the temperature decreases. Khan *et al.* [33] explored the dynamics of micropolar fluids within porous channels through a semi-analytical approach, focusing on the behaviors of fluids with micropolar characteristics and their interactions with porous structures. In studies of Hasegan *et al.*, Mihai *et al.*, Boicean *et al.*, Pirvut *et al.*, and Dawar *et al.* [20,21,34–36] the behavior of chemically reactive MHD flow in micropolar NFs was investigated. The researchers conducted a focused investigation on the impacts of velocity slips and fluctuations in the heat source/sink. The study demonstrated several applications, such as wire drawing, liquid composite molding, metal spinning, gas blowing, extrusion of polymer sheets, and manufacture of hot rolling and plastic films. Sakiadis [37] presented the results of a study investigating the characteristics of fluid flow over a solid border under constant conditions. Tsou *et al.* [38] explored the heat transfer onto a stretched sheet, and Crane [39] inspected an analytical solution for the flow of a viscous fluid generated by a surface that is linearly stretched. In their study, Gupta and Gupta [40] examined the impact of linear velocity on a flexible sheet while also considering the effects of suction or blowing. Grubka and Bobba [41] employed linear velocity in their investigation of heat transfer characteristics under different temperature distributions.

The flow of blood through arteries is a fundamental part of the cardiovascular system, responsible for distributing oxygen-rich blood from the heart to various tissues and organs throughout the body, which is not only crucial for the delivery of essential nutrients and oxygen but also plays a significant role in the removal of waste products and carbon dioxide. Recent work on blood through arteries includes the study of Das *et al.* [42] who examined the effects of Hall currents on blood flow through mildly stenosed, inclined arteries using a homotopy perturbation method, while Karmakar *et al.* [43] investigated the dynamics of blood containing trihybrid nanoparticles pumped through an eccentric endoscopic arterial canal using an electro-osmotic mechanism, which enhanced the understanding of targeted drug delivery systems within complex vascular architectures. More recently, Ali and Das [44] applied neuro-computing and fractional calculus to analyze blood flow carrying modified trihybrid nanoparticles in a diseased ciliated artery, and Paul *et al.* [45] demonstrated the use of a balloon catheter for angioplasty in arteries containing a tetra-hybrid nano-bloodstream under a magnetic field, analyzed *via* artificial neural networks, and their work contributes to the development of precision interventions in cardiology, particularly in magnetically influenced environments.

Fluid flow over curved surfaces is a highly intriguing subject in the field of fluid mechanics, having a wide range of practical uses in areas such as aerospace engineering and biomedical devices. When a fluid moves across a curved surface, various significant phenomena arise because of the interaction between the fluid and the curvature of the surface. Given the significance and practical relevance of fluid flow over curved surfaces, it has garnered considerable attention in the literature. Haq *et al.* [46] explored periodic heat transfer through extended surfaces, shedding light on the periodic nature of heat transfer processes and its implications for optimizing thermal management across diverse applications. A study conducted by Ahmed and Khan [47] investigated the causes of fluid flow on a curved surface with pores incorporating magneto-nanomaterials. Sheikholeslami *et al.* [48] formulated a

mathematical model to describe the fluid flow of nanomaterials when employing MHD on an inclined surface. Additionally, Ahmed and Khan [44] conducted research in this area. Computational modeling of MHD flow of the Sisko NF past a curved surface in motion.

The aim of this work is to examine the characteristics of magnetized micropolar blood including Cu and gold (Au) nanoparticles in an HNF as it moves across a curved surface. This work demonstrates innovation and originality by integrating the following concepts:

- Unsteady flow.
- Magnetized micropolar blood-based NF.
- An HNF that incorporates both Cu and Au nanoparticles.
- Consideration of complicated geometry with curved surfaces.
- The study examines different factors, including the Prandtl number, volume proportion of nanoparticles, and blood flow parameters.

The present study uniquely integrates MHD and micropolar fluid dynamics with HNFs in a medically relevant model of blood flow through stenotic arteries. Unlike previous studies, such as the exploration of HNF heat transfer over different geometries by Ashwinkumar *et al.* [10] or the experimental analysis of Au–blood NF flow in stenotic arteries by Sarwar and Hussain [13], this study introduces a comprehensive framework for modeling blood flow under the simultaneous influence of magnetic fields, slip effects, and porous stenosis conditions. Building on the foundational theory of micropolar fluids established by Eringen [15], it incorporates advanced numerical methods to capture the unsteady behavior of HNFs (blood–Au + TiO_2), revealing significant improvements in heat transfer and flow dynamics. Additionally, the thermal performance findings of Waini *et al.* [9] and the axisymmetric flow explored by Nadeem *et al.* [6] are extended to address curved, porous surfaces, with specific attention to the implications for cardiovascular treatments. By unifying these elements, the current work advances the understanding of HNF dynamics in biomedical applications, offering new insights into optimizing drug delivery and managing arterial disorders. Additionally, Table 1 explains the novelty with reference to the available literature.

1.1 The investigation progresses in a systematic manner

First, the governing equations are solved with great attention to detail, resulting in a numerical solution achieved with MATLAB software. Afterward, a detailed representation of the physical measurements linked to various parameters is given by displaying graphs. The results of this research are highly relevant to a wide range of biomedical applications.

2 Formulation

2.1 Geometry and physical description of the model

The 2D flow model of a micropolar time-dependent hybrid magnetized NF moving through a stenosis artery is scrutinized in the present study context. We considered that blood flowing through an artery stenosis of length $\frac{L_0}{2}$ behaves like an incompressible unsteady Newtonian micropolar fluid flow. The blood flow is assumed to be along the x-axis and perpendicular to the r-axis. The artery has a cosine-shaped stenosis having a width of unobstructed region of $2R_{0_o}$, where $R(x)$ is the artery's radius

Table 1: Comparative summary of key features addressed in previous and current studies on hybrid nanofluid and methods applied

References	MHD HNF	Blood-based NF	Micropolar dynamics	Heat transfer	Numerical methods	Experimental methods	Medical relevance
Ashwinkumar *et al.* [10]	✓	✗	✗	✓	✓	✗	✓
Sarwar and Hussain [13]	✓	✓	✗	✓	✓	✓	✓
Waini *et al.* [9]	✓	✗	✗	✓	✓	✗	✓
Ghalambaz *et al.* [29]	✓	✗	✗	✓	✓	✗	✓
Nadeem *et al.* [6]	✗	✗	✓	✗	✓	✗	✓
Eringen [15]	✗	✗	✓	✗	✗	✗	✗
Current study	✓	✓	✓	✓	✓	✗	✓

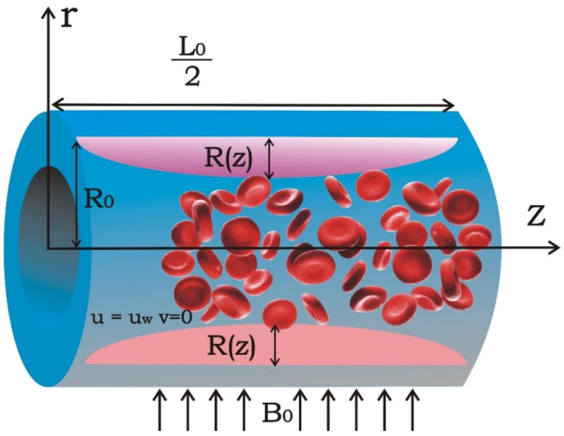

Figure 1: Geometrical demonstration of the problem.

which is the stenosis's greatest height. The following profile is adopted for the stenosed area (Figure 1) [13,45]:

$$R(x) = R_0 - \frac{\lambda}{2}\left(1 + \cos\left(\frac{4\pi x}{L_0}\right)\right), \quad -\frac{L_0}{4} < x < \frac{L_0}{4} = R_0, \text{ Otherwise}, \tag{1}$$

2.2 Assumptions

- Blood behaves as a micropolar fluid with inherent microstructural behaviors.
- The flow is unsteady, with varying flow characteristics over time.
- The fluid is a magnetically influenced HNF.
- Blood flow is assumed incompressible, maintaining constant density under pressure variations.
- Artery stenosis is modeled with a cosine-shaped profile for precise geometric simulation.
- Blood flow is directed along the x-axis and perpendicular to the r-axis, simplifying the analysis to two dimensions.
- Incorporates gyration tensor, micro-inertia, and microstress in the fluid's constitutive equations, reflecting complex internal and magnetic interactions.

2.3 Mathematical modeling

The vector form of the constitutive equations which describe the micropolar nature of the fluid is written by combining novel kinematic features, such as the gyration tensor and the micro-inertia, moment tensor, as well as the thoughts of micro-stress, body, and stress moments. These equations also consider the magnetic effect as follows [13,46]:

$$\nabla \cdot \boldsymbol{V} = 0, \tag{2}$$

$$\rho_f\left(\frac{\partial \boldsymbol{V}}{\partial t} + \boldsymbol{V}\cdot\nabla\boldsymbol{V}\right) = -\nabla\, \mathrm{p} + (\mu_f + k^*)\nabla^2\boldsymbol{V} + k^*(\nabla \times \mathbf{v}) + \mu\frac{u}{K} + \rho_f F u^2 + \boldsymbol{J}\times\boldsymbol{B}, \tag{3}$$

$$\rho_f j\left(\frac{\partial \mathbf{v}}{\partial t} + \mathbf{v}\cdot\nabla\mathbf{v}\right) = (\alpha + \beta + \gamma)\nabla\cdot\nabla\mathbf{v} - \gamma(\nabla\times\nabla\times\mathbf{v}) + k^*(\nabla\times\mathbf{v}) - 2k\mathbf{v} + \boldsymbol{J}\times\boldsymbol{B}. \tag{4}$$

The inequalities are as follows [45]:

$$k \geq 0,\ 2\mu_{\mathrm{f}} + k \geq 0,\ 3\alpha + \beta + \gamma \geq 0,\ |\gamma| \geq \beta.$$

The thermal energy and nanoparticle diffusion equations, which adhere to the Fourier and Fick laws, are expressed in accordance with Buongiorno's model [13].

$$\rho_{\mathrm{f}} c_{\mathrm{f}}\left(\frac{\partial T}{\partial t} + \boldsymbol{V}\cdot\nabla T\right) = k_{\mathrm{f}}\nabla^2 T. \tag{5}$$

Here, ρ_{f} and c_{f} refer to the density and specific heat of nanoparticles, respectively. The variables in the given equation are given in Table 2.

2.4 Reduced equations after implementation of assumptions and boundary conditions

The equations that regulate the flow and heat transfer for Newtonian NFs in an unstable boundary layer are defined, assuming certain conditions [13,46]

$$\frac{\partial}{\partial x}(ru) + \frac{\partial}{\partial r}(rv) = 0, \tag{6}$$

$$\frac{\partial u}{\partial t} + u\left(\frac{\partial u}{\partial x}\right) + v\left(\frac{\partial u}{\partial r}\right) = \frac{(\mu_{\mathrm{hnf}} + k^*)}{\rho_{\mathrm{hnf}}}\frac{\partial}{r\partial r}\left(r\frac{\partial u}{\partial r}\right) - \frac{\sigma_{\mathrm{hnf}}B_0^2}{\rho_{\mathrm{hnf}}}u - \frac{\mu_{\mathrm{hnf}}}{k_1}u - \frac{c_b}{\sqrt{k_1}}(u^2), \tag{7}$$

$$\frac{\partial N}{\partial t} + u\left(\frac{\partial N}{\partial x}\right) + v\left(\frac{\partial N}{\partial r}\right) = -\frac{\gamma^*}{j\rho_{\mathrm{hnf}}}\left(\frac{1}{r}\frac{\partial N}{\partial r} + \frac{\partial^2 N}{\partial r^2}\right) - \frac{k^*}{j\rho_{\mathrm{hnf}}}\left(\frac{\partial u}{\partial r} + 2N\right), \tag{8}$$

$$\frac{\partial T}{\partial t} + u\left(\frac{\partial\, T}{\partial x}\right) + v\left(\frac{\partial T}{\partial r}\right) = \frac{k_{\mathrm{hnf}}}{(\rho C_{\mathrm{p}})_{\mathrm{hnf}}}\left(\frac{\partial}{r\partial r}\left(r\frac{\partial T}{\partial r}\right)\right) + \frac{(\mu_{\mathrm{hnf}} + k^*)}{(\rho C_{\mathrm{p}})_{\mathrm{hnf}}}\left(\frac{\partial u}{\partial r}\right)^2 + \frac{\sigma_{\mathrm{hnf}}B_0^2}{(\rho C_{\mathrm{p}})_{\mathrm{hnf}}}u^2. \tag{9}$$

Table 2: Variables used

Parameter	Symbol
Velocity vector	$V = (u,\ v,\ w)$
Pressure	p
Microrotation	N
Current density	$J = \sigma_e(V \times B)$
Electrical conductivity	σ_e
Magnetic field	B
Fluid density	ρ_f
Dynamic viscosity	μ_f
Vortex viscosity	κ
Microinertia density	j
Gyroviscosity coefficients	α, β, γ
Temperature	T
Specific heat	c_f
Thermal conductivity	k_f
Density nanoparticles	ρ_p
Specific heat of nanoparticles	c_p

For this model, the workable boundary conditions are [13]

$$u = u_0,\ v = 0,\ N = N_0 \text{ and } T = T_0 \text{ at } r = R(x),$$
$$\frac{\partial u}{\partial r} = 0,\ \frac{\partial N}{\partial r} = 0,\ \text{and } \frac{\partial T}{\partial r} = 0,\ \text{as } r = 0. \tag{10}$$

2.5 Hybrid nanomaterial properties

To accurately forecast the heat transmission characteristics of NFs, a thorough examination of their thermophysical properties is essential. Nanoparticles can significantly improve heat conductivity compared to larger particles in suspension, such as millimeter-sized and micrometer-sized particles. Empirical research has shown that the thermal conductivity of NFs is affected by various elements, such as the temperature, the composition of the base fluid, the percentage of particle volume, the material composition of the particles, the size of the particles, and the form of the particles. The influence of NF additions on the improvement of heat conductivity has been found to be dependent on their features, such as kind, amount, and acidity. The thermo-physical characteristics and relationship of nano and hybrid nanomaterials are shown in Tables 3 and 4, respectively. Diagrams for the preparation and factors influencing the HNFs and application of Au and titanium dioxide (TiO_2) are given in Figure 2.

Table 3: Thermo-physical attributes of both the base fluid and the HNF $\Phi_1 + \Phi_2 = \Phi$ analyzed and reported in detail in previous studies [24–26]

Components	$c_p\left(\frac{J}{kg\,K}\right)$	$k\left(\frac{W}{m\,K}\right)$	$\sigma\left(\frac{m\,S}{m}\right)$	$\rho\left(\frac{kg}{m^3}\right)$
Gold (Au)	129	318	4.1×10^6	19,300
Titanium dioxide (TiO_2)	4,250	8.9538	6.27×10^{-5}	686.20
Blood	3,594	0.492	6.67×10^{-1}	1,063

2.6 Similarity transformation

Similarity transformation is a technique used to simplify the solution of partial differential equations (PDEs) by identifying scaling properties that allow the equations to be transformed into a dimensionless form. The principle behind similarity transformations lies in recognizing that certain physical systems or phenomena exhibit self-similarity. We use similarity transformation to reduce the given modeled equation. The appropriate transformations of similarity are specified as follows:

$$\begin{aligned} u &= \frac{a}{(1-at)}\frac{u_0 x}{L_0}F'(\eta),\ v = -\frac{R}{r}\sqrt{\frac{u_0\vartheta_f a}{L_0(1-at)}}F(\eta),\\ \eta &= \frac{r^2-R^2}{2R}\sqrt{\frac{u_0 a}{\vartheta_f L_0(1-at)}},\\ \theta(\eta) &= \frac{a}{(1-at)}\frac{T-T_\infty}{T_w-T_\infty},\ \text{and}\\ N &= u_0 a x\sqrt{\frac{u_0 a}{\vartheta_f L_0(1-at)}}g(\eta). \end{aligned} \tag{11}$$

2.7 Non-dimensional system of ordinary differential equations (ODEs)

After introducing similarity transformation, the following transformed governing equations are obtained.

$$\begin{aligned} &\frac{(\mu_{hnf}+K)}{\mu_f}((1+2\eta\gamma)f''' + 2\gamma f'')\\ &\quad - \frac{\rho_{hnf}}{\rho_f}\left(S\left(\frac{1}{2}\eta f'' + f'\right) + (f'^2 - ff'')\right) - \frac{\mu_{hnf}}{\mu_f}\beta_0 f'\\ &\quad - F_r f'^2 - \frac{\sigma_{hnf}}{\sigma_f}Mf' = 0, \end{aligned} \tag{12}$$

$$\begin{aligned} &S(\eta g' + g) + f'g - fg' + \frac{\rho_f}{\rho_{nf}}(1+K)((1+2\eta\gamma)g''\\ &\quad + 2\gamma g') + \frac{\rho_f}{\rho_{nf}}K((1+2\eta\gamma)^{1/2}f'' + 2Bg) = 0, \end{aligned} \tag{13}$$

$$\begin{aligned} &\frac{K_{nf}}{K_f}[(1+2\eta\gamma)\theta'' + 2\gamma\theta'] + \frac{(\mu_{hnf}+K)}{\mu_f}\mathrm{Pr}\,\mathrm{Ec}(1\\ &\quad + 2\eta\gamma)f''^2 + \frac{\sigma_{nf}}{\sigma_f}M\mathrm{Pr}\,\mathrm{Ec}(1+2\eta\gamma)f''^2\\ &\quad - \mathrm{Pr}\frac{(\rho C_p)_{nf}}{(\rho C_p)_f}[S(\eta\theta' - \theta) - f\theta'] = 0. \end{aligned} \tag{14}$$

Table 4: Thermo-physical interactions of NFs and HNFs [46]

Properties	NF and HNF
Viscosity	$\frac{\mu_{\text{hnf}}}{\mu_{\text{bf}}} = \frac{1}{(1-\phi_g-\phi_{\text{TiO}_2})^{2.5}}$
Density	$\frac{\rho_{\text{hnf}}}{\rho_{\text{bf}}} = \phi_g\left(\frac{\rho_g}{\rho_{\text{bf}}}\right) + \phi_{\text{TiO}_2}\left(\frac{\rho_{\text{TiO}_2}}{\rho_{\text{bf}}}\right) + (1 - \phi_g - \phi_{\text{TiO}_2})$
Thermal capacity	$\frac{(\rho c_{\text{p}})_{\text{hnf}}}{(\rho c_{\text{p}})_{\text{bf}}} = \phi_g\left(\frac{(\rho c_{\text{p}})_g}{(\rho c_{\text{p}})_{\text{bf}}}\right) + \phi_{\text{TiO}_2}\left(\frac{(\rho c_{\text{p}})_g}{(\rho c_{\text{p}})_{\text{bf}}}\right) + (1 - \phi_g - \phi_{\text{TiO}_2})$
Thermal conductivity	$\frac{k_{\text{hnf}}}{k_{\text{bf}}} = \frac{\frac{(\phi_g k_g + \phi_{\text{TiO}_2} k_{\text{TiO}_2})}{\phi_g + \phi_{\text{TiO}_2}} + \left\{\begin{matrix} 2k_{\text{bf}} + 2(\phi_g k_g + \phi_{\text{TiO}_2} k_{\text{TiO}_2}) - \\ 2(\phi_g + \phi_{\text{TiO}_2}) k_{\text{bf}} \end{matrix}\right\}}{\frac{(\phi_g k_g + \phi_{\text{TiO}_2} k_{\text{TiO}_2})}{\phi_g + \phi_{\text{TiO}_2}} + \left\{\begin{matrix} 2k_{\text{bf}} - (\phi_g k_g + \phi_{\text{TiO}_2} k_{\text{TiO}_2}) + \\ (\phi_g + \phi_{\text{TiO}_2}) k_{\text{bf}} \end{matrix}\right\}}$
Electrical conductivity	$\frac{\sigma_{\text{hnf}}}{\sigma_{\text{bf}}} = \frac{\frac{(\phi_g \sigma_g + \phi_{\text{TiO}_2} \sigma_{\text{TiO}_2})}{\phi_g + \phi_{\text{TiO}_2}} + \left\{\begin{matrix} 2\sigma_{\text{bf}} + 2(\phi_g \sigma_g + \phi_{\text{TiO}_2} \sigma_{\text{TiO}_2}) - \\ 2(\phi_g + \phi_{\text{TiO}_2}) \sigma_{\text{bf}} \end{matrix}\right\}}{\frac{(\phi_g k_g + \phi_{\text{TiO}_2} k_{\text{TiO}_2})}{\phi_g + \phi_{\text{TiO}_2}} + \left\{\begin{matrix} 2\sigma_{\text{bf}} - (\phi_g \sigma_g + \phi_{\text{TiO}_2} \sigma_{\text{TiO}_2}) + \\ (\phi_g + \phi_{\text{TiO}_2}) \sigma_{\text{bf}} \end{matrix}\right\}}$

The non-dimensional boundary conditions are as follows:

$$f(0) = 0, f'(0) = g(0) = \theta(0) = 1, \quad f''(\eta) = 0,\ g'(\eta) = \theta'(\eta) = 0 \text{ at } \eta = f. \tag{15}$$

2.7.1 Obtained physical parameters

The dimensionless parameters after modeling in Eqs. (12)–(15) are given with details in Table 5.

3 Calculation of physical quantities

The Nusselt number is a dimensionless parameter which is used in heat transfer analysis to describe the convective heat transfer between a fluid and a solid surface. It represents the ratio of convective heat transfer to conductive heat transfer over the thermal boundary layer. The Nusselt number essentially indicates the efficiency of convective heat transfer relative to conductive heat transfer. A higher Nusselt number signifies a higher convective heat transfer rate relative to conduction, indicating more efficient heat transfer. The Nusselt number is used to design and optimize heat exchangers, cooling systems, and other thermal devices.

Skin friction is another primary concept in the study of fluid flow. Skin friction refers to the drag force exerted by the fluid on a solid surface due to viscous shear stresses within the boundary layer. It is essential in various engineering applications, including hydrodynamics, aerodynamics, and heat transfer. The skin friction coefficient depends on the flow conditions, geometry of the surface, and properties of the fluid. Skin friction plays a role in convective heat transfer, particularly in forced convection where fluid flow over a surface enhances heat transfer. Comprehension and precise calculation of skin friction are essential for designing efficient vehicles, aircrafts, ships, and other structures where minimizing drag is crucial for performance and fuel efficiency. The physical quantities, *i.e.*, skin friction coefficient C_{f} and heat transfer coefficient Nu of the flow field are defined as:

$$C_{\text{f}} = \frac{\tau_w}{\frac{1}{2}\rho_{\text{f}} U_w^2}, \ \text{Nu} = \frac{x q_w}{k_f (T_w - T_\infty)}, \tag{16}$$

where shear stress τ_w and q_w are

$$\tau_w = \frac{(\mu_{hnf} + K)}{\mu_f} \frac{\partial u}{\partial r}\bigg|_{r=R}, \ \text{Re}_x^{1/2} C_f = \frac{(\mu_{\text{hnf}} + K)}{\mu_{\text{f}}} F''(0). \tag{17}$$

$$q_w = -k_{\text{hnf}} \frac{\partial T}{\partial r}\bigg|_{r=R}, \ \text{Re}_x^{1/2} \text{Nu}_x = -\frac{k_{\text{hnf}}}{k}(\theta'),$$

where $\text{Re}_x^{-1/2}$ is the local Reynolds number.

4 Solution methodology

In this section, the solution procedure for this model is determined by using a shooting method with the bvp4c solver. The model's ODEs are numerically solved using the MATLAB tool's bvp4c solver, which uses a shooting strategy. The first step in using this method is to convert the higher-order system into a first-order system. To

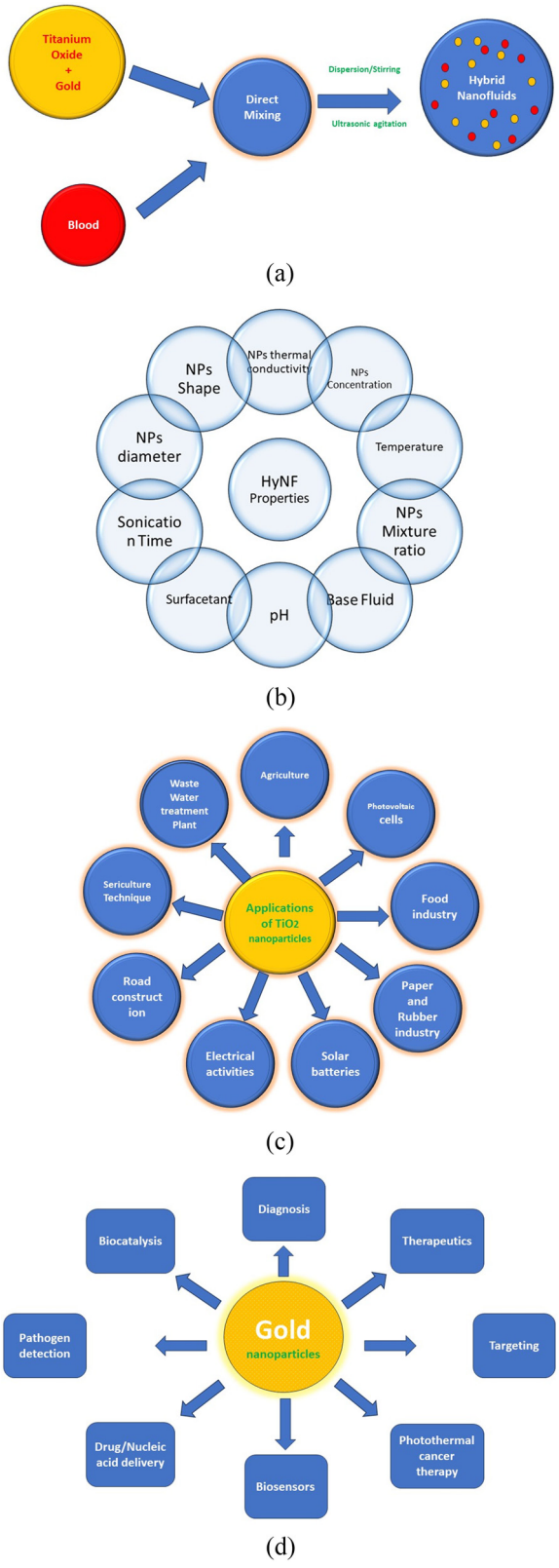

Figure 2: (a) Diagram for the preparation of HNFs. (b) Factors impacting the HNF properties. (c) Application of TiO_2. (d) Applications of Au nanoparticles.

complete this conversion, several guidelines will be followed:

$$f = y_1,\ f' = y_2, f'' = y_3,\ g = y_4,\ g' = y_5,\ y_6 = \theta,\ y_7 = \theta', \tag{18}$$

$$y_3' = -\frac{2\gamma}{1+2\eta\gamma}y_3 + \frac{1}{(1+2\eta\gamma)D_1}\left[D_2\left\{S\left(\frac{1}{2}\eta y_3 + y_2\right) + (y_2^2 - y_1y_3)\right\} + (D_1\beta_0 + D_5M)y_2 + Fyy_2^2\right], \tag{19}$$

$$y_5' = -\frac{2\gamma}{1+2\eta\gamma}y_5 - \frac{1}{(1+K)(1+2\eta\gamma)}[D_2\{S(\eta y_5 + y_4) + y_2y_4 - y_1y_5\} + K(1+2\eta\gamma)^{1/2}y_3 + 2By_4], \tag{20}$$

$$y_7' = -\frac{2\gamma}{1+2\eta\gamma}y_7 + \frac{1}{D_4(1+2\eta\gamma)}[\mathrm{Pr}D_3(S(\eta y_7 - y_6) - y_1y_7) - D_1PrEc(1+2\eta\gamma)y_3^2 - D_5\mathrm{Pr}\ \mathrm{Ec}M(1+2\eta\gamma)y_3^2]. \tag{21}$$

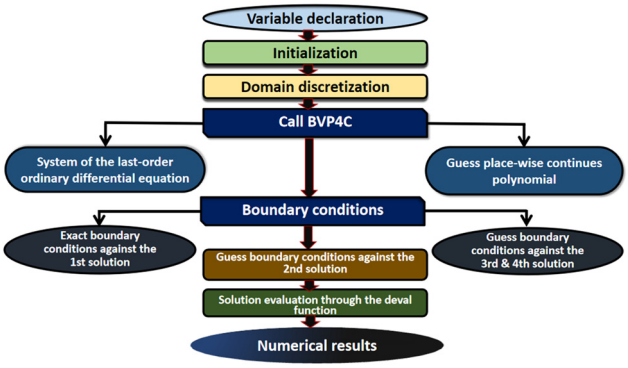

Table 5: Physical parameters and details

Parameter	Symbol	Mathematical form
Micropolar material parameter	K	$K = \frac{K^*}{\mu_f}$
Micro-inertia density parameter	B	$B = \frac{\vartheta_f(1-at)L_0}{au_0 j}$
Coefficient of inertia	F_r	$F_r = \frac{Fx}{\rho_f} = \frac{C_b x}{\sqrt{k}\rho_f}$
Unsteady parameter	S	$S = \frac{aL_0}{au_0}$
Curvature parameter	γ	$\gamma = \frac{L_0(1-at)\vartheta_f}{u_0 aR^2}$
Eckert number	Ec	$\mathrm{Ec} = \frac{u_0^2 a^3 x^2}{(1-at)^2 L_0^2 C_p(T_w - T_\infty)}$
Prandtl number	Pr	$\mathrm{Pr} = \frac{k_f}{(\mu C_p)_f}$
Magnetic parameter	M	$M = \frac{\sigma_f B_0^2 L_0(1-at)}{\rho_f a u_0}$
Porosity parameter	β_0	$\beta_0 = \frac{\mu_f L_0(1-at)}{\rho_f a u_0 K}$

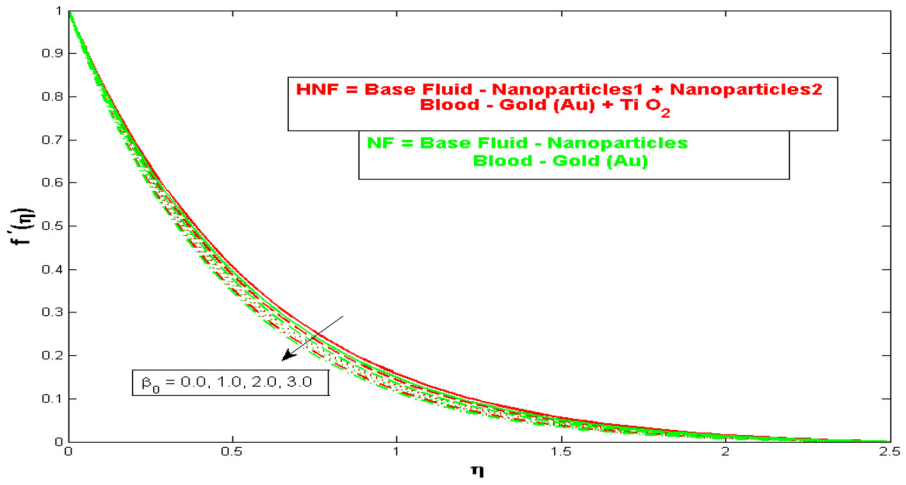

Figure 3: Effects of porosity parameter β_0 on the velocity profile $f'(\eta)$ for both the HNF (blood–Au + O_2) and NF (blood–Au).

5 Results and discussion

This study presents a detailed scrutiny of the impact of heat generation on the unsteady magnetized micropolar blood-based HNF flow through a porous stenotic artery. The bvp4c method was used to compute results numerically in a nonlinear system. To attribute influential parameters on velocity, microrotation and temperature profiles are examined in this section.

5.1 Velocity profile

Figure 3 indicates the effects of the β_0 porosity parameter on $f'(\eta)$ for the HNF (blood–Au + TiO_2) and the NF (blood–Au). It is observed that $f'(\eta)$ decreases for both fluids as the porosity parameter increases. This is attributed to the fact that introducing more pores on the porous surface creates additional resistance to fluid flow. The velocity behavior is almost the same for both NFs which is clearly reflected in the graph. Figure 4 showcases the relation between the coefficient of inertia F_r and velocity profile $f'(\eta)$. When the coefficient of inertia F_r is increased, the velocity decreases for both the HNF and NF because the fluid's resistance to acceleration or velocity changes may rise with a higher coefficient of inertia. In regions where the flow is changing, this higher resistance may cause a drop in the overall velocity profile. Variations in this coefficient can have an impact on the equations' acceleration terms, which in turn can have an impact on the velocity profile. Higher inertia coefficients increase resistance to

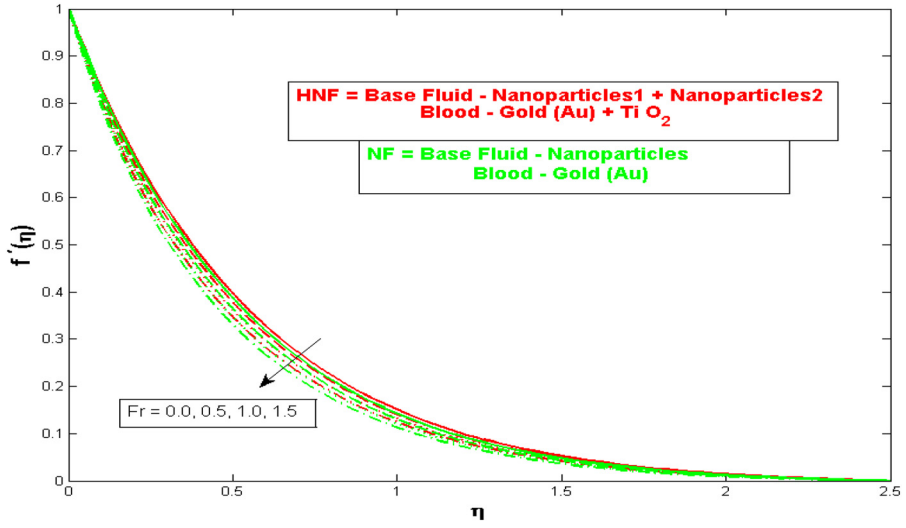

Figure 4: Influence of the coefficient of inertia F_r on the velocity profile $f'(\eta)$ for the HNF (blood–Au + TiO_2) and NF (blood–Au).

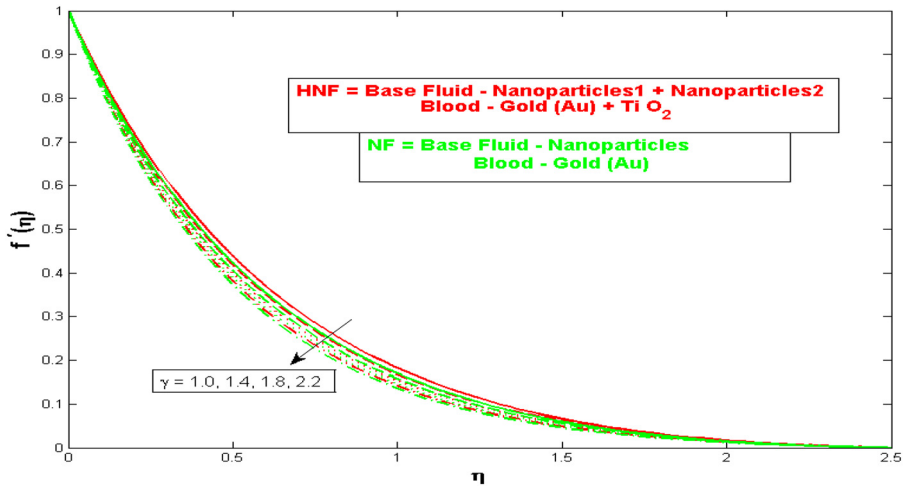

Figure 5: Impact of the curvature parameter γ on the velocity profile $f'(\eta)$.

changes in motion, thus decreasing velocity as the fluid struggles to accelerate. Figure 5 illustrates the effect of curvature parameter γ on the velocity profile $f'(\eta)$. The velocity declines for increasing values of curvature parameter γ because centripetal acceleration is a factor in fluid flow along a curved surface. This acceleration is aimed at the center of curvature and acts perpendicular to the velocity direction. The centripetal acceleration rises with increasing curvature, causing the total velocity to decrease. Increased curvature enhances centripetal forces acting perpendicular to the flow, reducing the velocity due to higher directional force requirements. Figure 6 portrays the influence of the micropolar material parameter K on the velocity profile $f'(\eta)$, that is, when the material parameter K increases, the micropolar velocity profile decreases for both the HNF and NF. The micropolar material parameter, often referred to as the spin gradient viscosity or microinertia, is represented by the parameter K in the context of micropolar fluid theory. It measures the impact of the fluid's microrotations. A rise in K indicates a corresponding increase in the fluid's microinertia, or resistance to micro-rotations. The fluid therefore becomes more resilient to internal deformations or small-scale rotating movements. This higher resistance has the tendency to restrict the micro-rotations, which has an impact on the fluid's overall velocity profile. Figure 7 depicts the relation between the magnetic parameter M and velocity profile; it can be noted that for higher values of magnetic

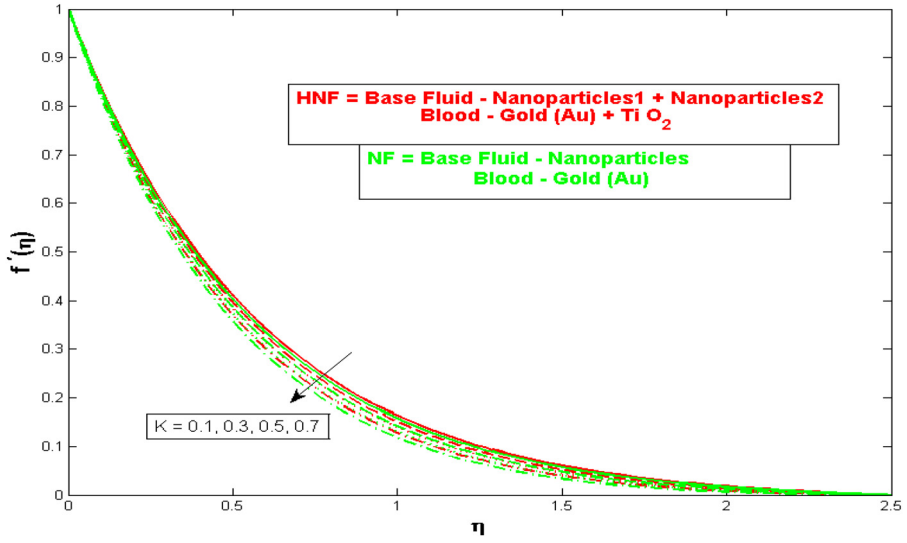

Figure 6: Variation of the velocity profile $f'(\eta)$ with the micropolar material parameter K for the HNF (blood–Au + TiO_2) and NF (blood–Au).

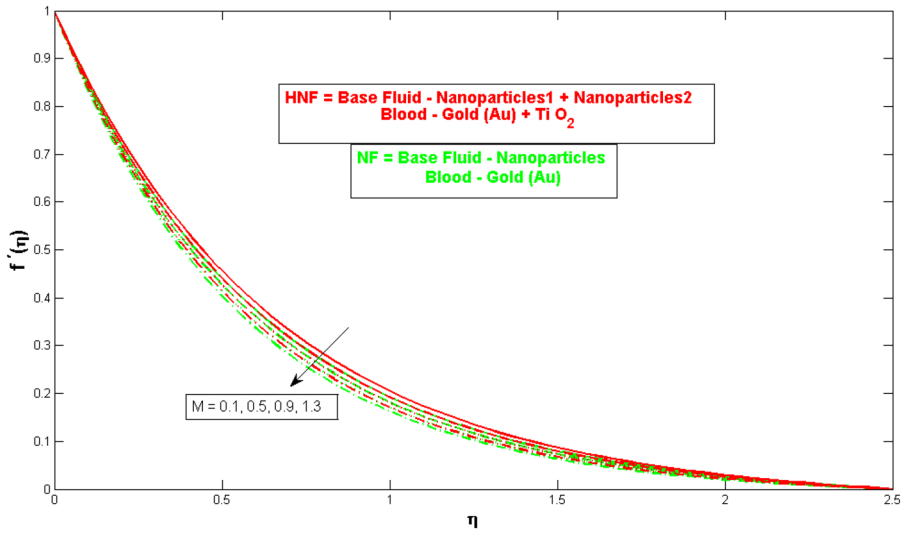

Figure 7: Relationship between the magnetic parameter M and the velocity profile $f'(\eta)$.

parameter M, the velocity profile decreases for both the HNF and NF because the Lorentz force is an important component of MHD. The interaction of the magnetic field with the fluid's generated electric currents produces this force. The fluid motion may encounter resistance from the Lorentz force, which would affect the velocity. In Figure 8, the impact of volume fraction ϕ on the velocity profile is displayed, and it is revealed that for increasing values of ϕ the velocity profile enhances for both the HNFs and NFs. This is due to the change in thermal as well as dynamic viscosity of the fluids. Also, the increasing value of ϕ enhances the concentration rate which further increases the fluid convection. This increasing trend of convection further increases the velocity profile. Particularly, when the volume fraction ϕ of TiO_2 nanoparticles is increased while maintaining the volume fraction ϕ of Au constant, the velocity profile in the HNF is observed to sharply increase. This observation implies that, under the given conditions, TiO_2 nanoparticles may have a more pronounced effect on fluid dynamics than Au nanoparticles. Figure 9 manifests the fluctuations between the value of ϕ and velocity profile $f'(\eta)$. When the volume fraction ϕ is augmented, the velocity profile increases for both the HNF and NF because the viscosity and thermal conductivity of the NF may both be improved by adding Au nanoparticles. While higher viscosity may have an impact on fluid flow and perhaps increase velocity dispersion, enhanced thermal conductivity can result in better heat transfer. It appears that Au nanoparticles under these circumstances have a greater influence on the flow dynamics than TiO_2 nanoparticles based on the observation that velocity increases by increasing the volume fraction ϕ of Au while

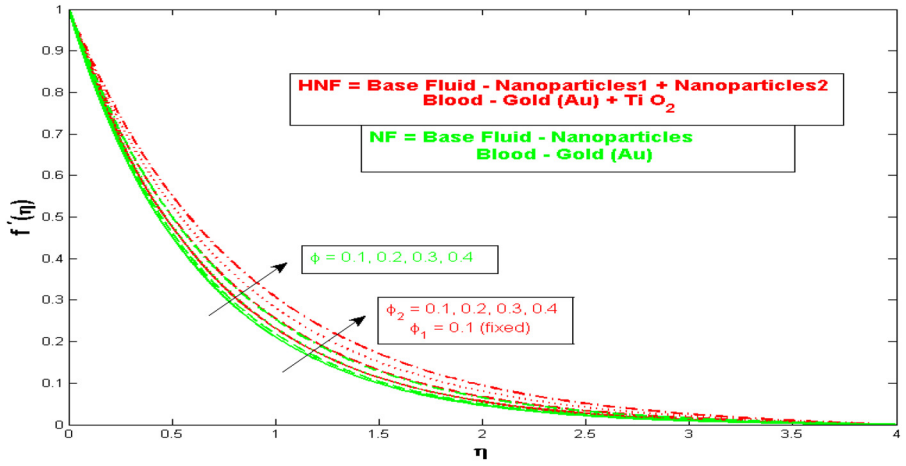

Figure 8: Effect of the volume fraction ϕ on the velocity profile $f'(\eta)$ for both the HNF (blood–Au + TiO_2) and NF (blood–Au).

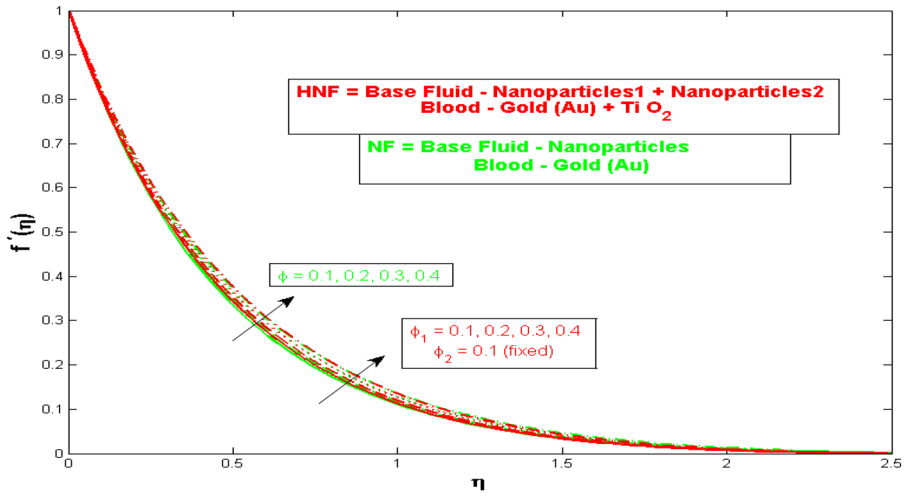

Figure 9: Influence of ϕ on the velocity for both the HNF (blood–Au + O_2) and NF (blood–Au).

maintaining the volume fraction ϕ of TiO_2 in the HNF. Figure 10 highlights the effects between the ϕ and velocity profile. It is observed that for the boosted volume fraction ϕ the velocity profile increases for both the HNF and NF because, among other things, the addition of nanoparticles to a fluid can change its viscosity and thermal conductivity. When the volume fraction ϕ increases, the concentration of nanoparticles in the fluid also increases. The fluid's behavior may alter because of this concentration increase, raising the velocity profile. Particularly, when the volume fraction ϕ of TiO_2 nanoparticles is increased while maintaining the volume fraction ϕ of Au constant, the velocity profile in the HNF is observed to sharply increase. This observation implies that, under the given conditions, TiO_2 nanoparticles may have a more pronounced effect on fluid dynamics than Au nanoparticles. Figure 11 exhibits the interdependence between the unsteady parameter S and velocity profile $f'(\eta)$. The velocity profile decreases for both the HNF and NF if the unsteady parameter S is increased because time-dependent variations in pressure and velocity are characteristics of unsteady flows. A higher level of unsteadiness in the flow is indicated by a rise in the unsteady parameter S. The velocity field may experience oscillations or changes as a result.

5.2 Temperature profile

It is recorded in Figure 12 that with the increase of the porosity parameter β_0, the temperature increases for both the HNF and NF because the fluid's and the porous medium's interaction can be affected by the porosity

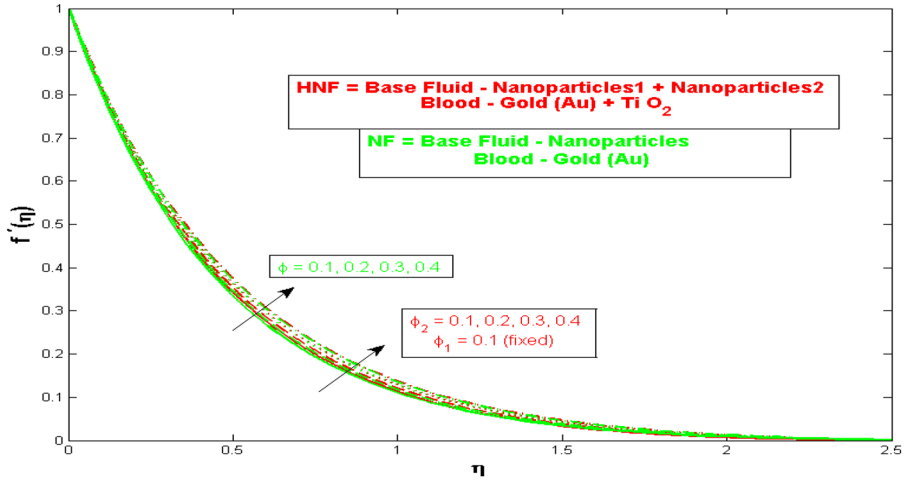

Figure 10: Variation of ϕ on the $f'(\eta)$ for the HNF (blood–Au + TiO_2) and NF (blood–Au).

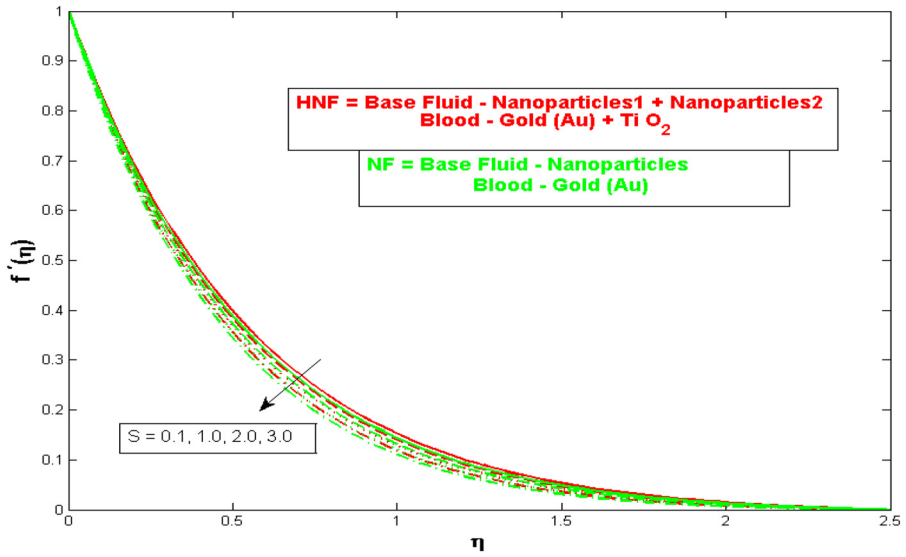

Figure 11: Variation of S on $f'(\eta)$ for the HNF (blood–Au + TiO_2) and NF (blood–Au).

parameter. Elevated temperature profiles may result from enhanced heat transfer between the fluid and solid due to a higher degree of contact between the fluid and the porous structure. The variation between the magnetic parameter M and temperature profile $\theta(\eta)$ is presented in Figure 13, and it is recognized that as fog enlarged the value of the magnetic parameter M the temperature profile increases for both the HNF and NF because the fluid's ability to transmit heat can be improved by the magnetic field. This is especially true for NFs in which the base fluid contains scattered nanoparticles (like Au). These nanoparticles' mobility may be influenced by the magnetic field, which can enhance heat conduction. The dominance of Ec on temperature profile $\theta(\eta)$ is shown in Figure 14; it is noted that the increment in the Ec causes an enhancement in the temperature for both the HNF and NF because an increase in the Ec indicates a higher kinetic energy relative to internal energy, which can lead to enhanced convective

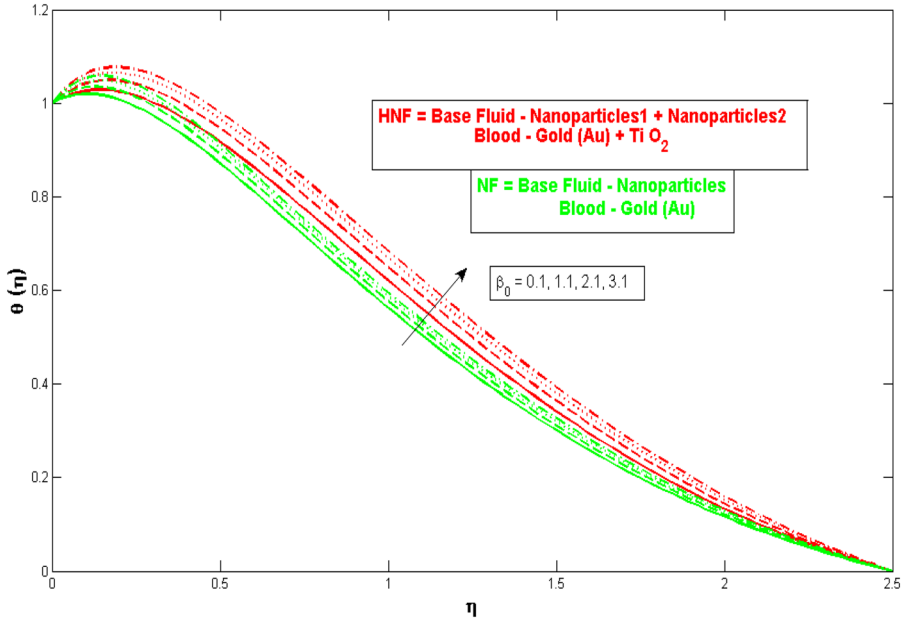

Figure 12: Effect of porosity parameter β_0 on temperature, showing an increase in temperature with higher porosity due to improved fluid–porous medium interaction.

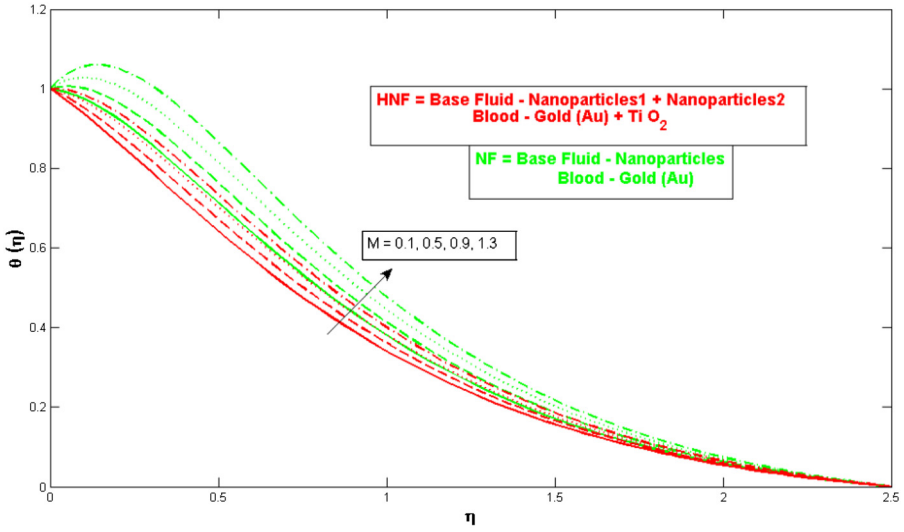

Figure 13: Influence of the magnetic parameter M on temperature.

heat transfer and higher temperature profiles. The Ec is frequently associated with the balance between kinetic energy and internal energy (enthalpy) in a fluid flow. With the increase in the curvature parameter γ, the temperature decreases for both the HNF and NF, which is shown in Figure 15, because heat conduction and convective heat transmission can be balanced differently depending on curvature changes. Heat transmission away from the surface may be improved by higher curvature due to greater convective processes. However, lower temperature profiles might arise if this improvement is insufficient to offset any decrease in heat conduction. Figure 16 displays the modification between the unsteady parameter S and temperature profile $\theta(\eta)$, which shows that with the increase in the unsteady parameter S the temperature increases for both the HNF and NF, because higher levels of unsteadiness in the flow are frequently indicated by a rise in the unsteady parameter. There might be more transient heat transfer processes because of this enhanced unsteadiness. Temperature variations can be caused by transient heat transfer, and under some circumstances the temperature profile may rise overall.

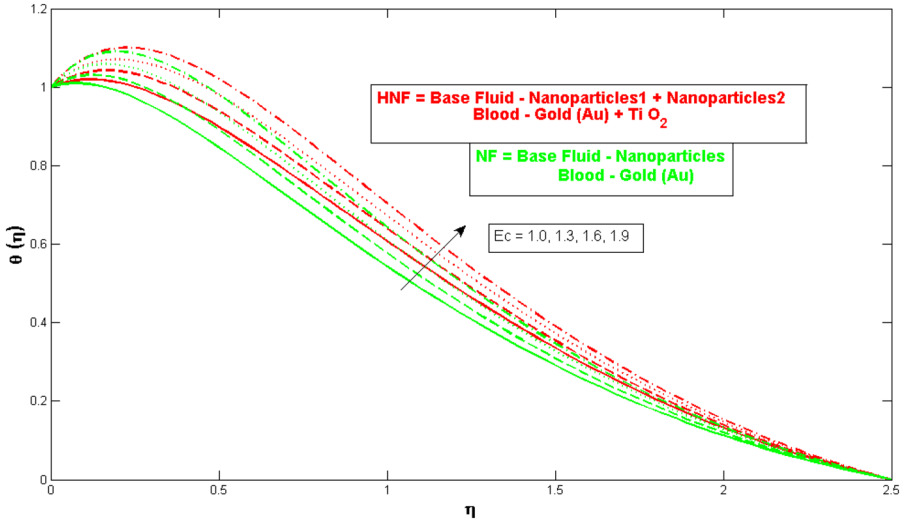

Figure 14: Effect of the Ec on temperature, indicating that higher Ec increases the temperature by enhancing convective heat transfer.

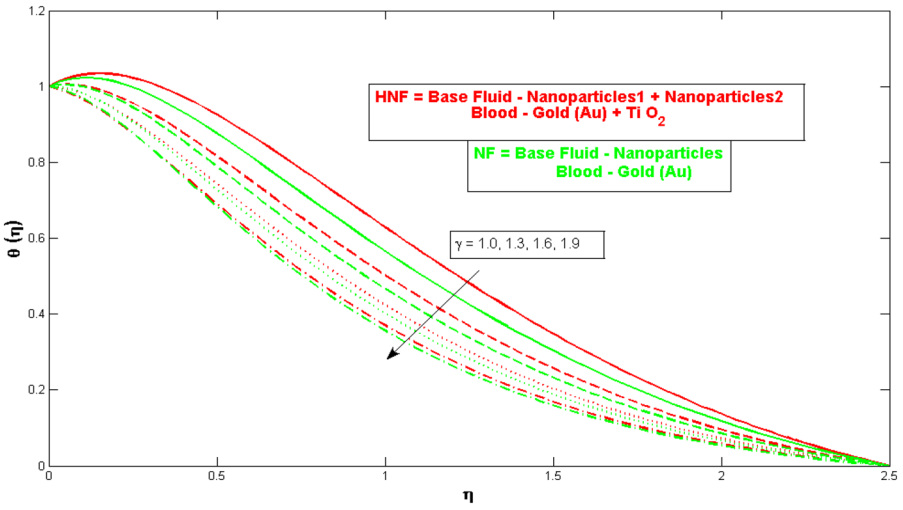

Figure 15: Influence of the curvature parameter *y* on temperature, showing a decrease in temperature with increasing curvature due to changes in heat transfer dynamics.

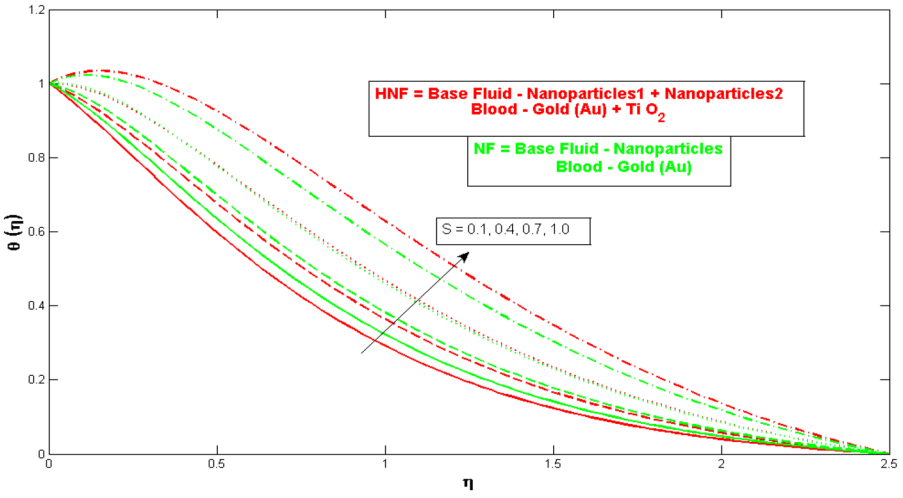

Figure 16: Impact of the unsteady parameter *S* on temperature, where an increase in *S* results in a higher temperature due to enhanced transient heat transfer.

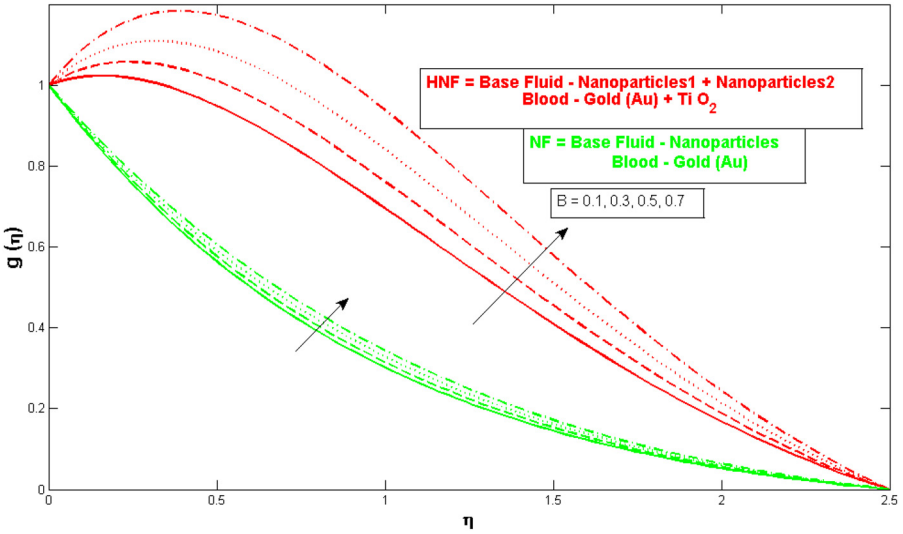

Figure 17: Effect of micro-inertia density parameter *B* on the micropolar profile $g(\eta)$, showing an increase in profile with higher *B* for both hybrid and conventional NFs.

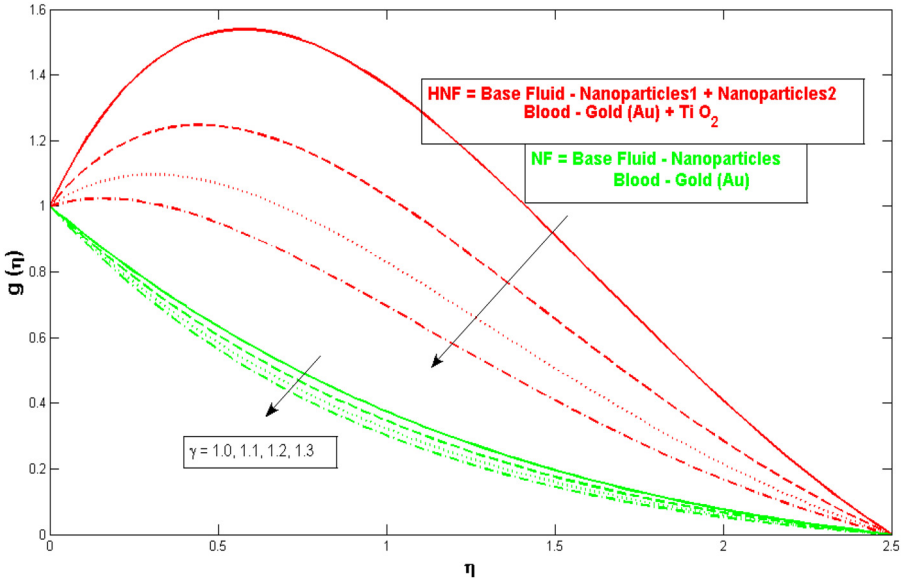

Figure 18: Influence of the curvature parameter γ on the micropolar profile $g(\eta)$.

5.3 Micro-rotation profile

Figure 17 demonstrates the control of the micro-inertia density parameter B on micropolar profile $g(\eta)$; with the increase of the micro-inertia density parameter B, the micropolar profile increases for both the HNF and NF because micro-inertia and nanoparticle dynamics may combine to provide a synergistic impact in an HNF that contains both micropolar effects and nanoparticles. In comparison to the conventional NF, the HNF may exhibit a greater rise in the micropolar profile due to the combined impact of micro-inertia and nanoparticle dispersion. Figure 18 highlights the variant linking the curvature parameter γ and micropolar profile $g(\eta)$. When the curvature γ is increased, the micropolar profile decreases for both the HNF and NF, because micro-rotation and micro-deformation effects are a result of the fluid's micropolar character. A decrease in the micropolar profile $g(\eta)$ can occur from modifications in the microstructure and flow patterns of the micropolar fluid caused by an increase in curvature γ. When the micropolar material parameter K is boosted, the micropolar profile decreases for both the HNF and NF as shown in Figure 19, because the degree of micro-deformation and micro-rotation in the fluid is characterized by the micropolar material parameter K. An increase in K can cause the fluid's micro-deformation and micro-

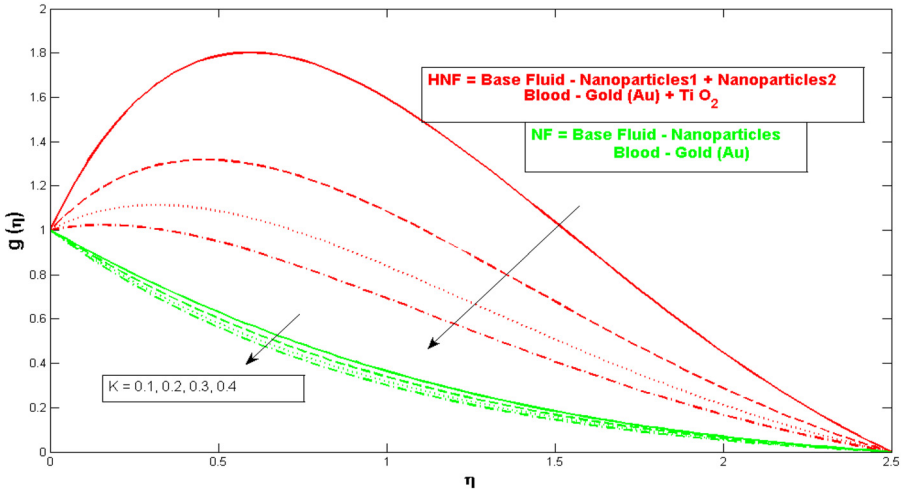

Figure 19: Impact of the micropolar material parameter K on the micropolar profile $g(\eta)$.

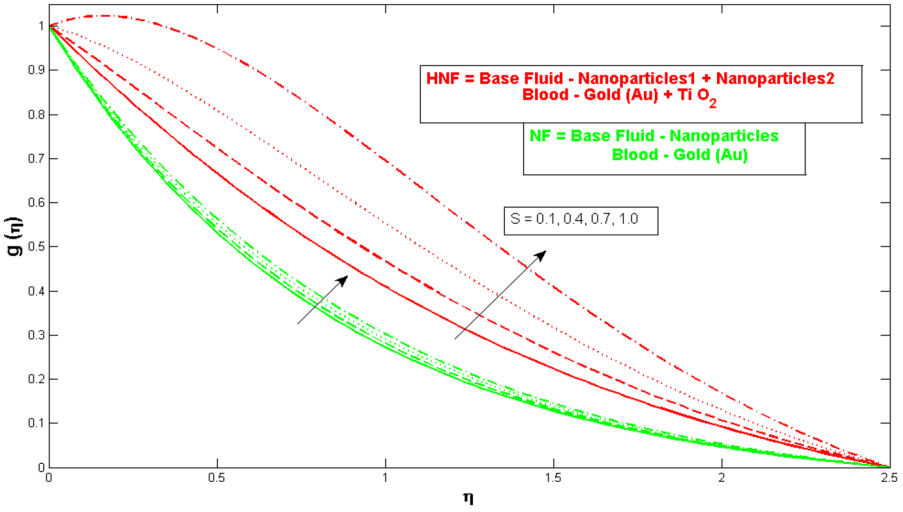

Figure 20: Effect of the unsteady parameter S on the micropolar profile $g(\eta)$.

rotation to rise, which can alter the flow patterns and concentration profiles and decrease the micropolar profile $g(\eta)$. The persuasion of the unsteady parameter S on micropolar profile $g(\eta)$ is displayed in Figure 20. When there is an increase in the unsteady parameter S, the micropolar profile increases for both the HNF and NF, because a more dynamic flow field is suggested by an increase in the unsteady parameter S. The micropolar profile $g(\eta)$ increases because of increased mixing and transport caused by unsteady flows.

Table 6 exhibits the values of skin friction coefficient for numerous parameters. It is noteworthy that the skin friction coefficient drops for large values of porosity, unsteady, magnetic, and flow parameters. Table 7 highlights how the various parameters and the Nusselt number are interdependent. It is recorded that the Nusselt number lowers for large values of porosity parameter, Eckert number, flow parameter and unsteady parameter. Table 8 shows a comparison with the already published work, which shows the validity of our results. The comparison is made for different values of the parameters γ (shear parameter) and ϕ (volume fraction of nanoparticles) in terms of the dimensionless friction factor. The close agreement between the results of the present study and those from the published work validates the accuracy and reliability of the current model.

6 Conclusions

In the present investigation, we developed a mathematical model to describe the unsteady magnetized flow of a

Table 6: Impact of different parameters on skin friction coefficient

β_0	S	γ	M	NF	HNF
0.10	0.10	0.10		−2.114507	−2.512631
0.20				−2.181286	−2.607065
0.30				−2.246348	−2.698726
0.1	0.1	0.1		−2.114507	−2.512631
	0.2			−2.240494	−2.659066
	0.3			−2.35676	−2.795233
0.1	0.1	0.1		−2.114507	−2.512631
		0.2		−2.198743	−2.634848
		0.3		−2.279811	−2.752537
			0.1	−2.114507	−2.512631
			0.2	−2.1593	−2.577853
			0.3	−2.203312	−2.641736

Table 7: Influence of some parameters on the Nusselt number

β_0	Ec	γ	S	NF	HNF
0.1	1.0	1.0	0.1	0.6531922	2.177478
0.2				0.6358387	2.153595
0.3				0.6187621	2.130125
0.1	1.0	1.0	0.1	0.6531922	2.177478
	1.1			0.5627625	2.063243
	1.2			0.4723327	1.949009
0.1	1.0	1.0	0.1	0.6531922	2.177478
		1.1		0.6807187	2.265521
				0.706238	2.34732
0.1	1.0	1.0	0.1	0.6531922	2.177478
			0.2	0.5178419	2.001518
			0.3	0.3775971	1.821829

Table 8: Comparison of γ and ϕ values in the present work and the literature

γ	ϕ	Present work $\mathrm{Re}_x^{1/2}\mathrm{Re}_x{}^{1/2}C_f$	Published work [13] $\mathrm{Re}_x^{1/2}\mathrm{Re}_x{}^{1/2}C_f$
0.1	0.0	−0.9352436	−0.939968
0.12		−0.9219889	−0.924794
0.14		−0.9099237	−0.911311
0.1	0.0	−0.9352436	−0.939968
	0.05	−1.324139	−1.329552
	0.1	−1.689456	−1.715985

micropolar fluid across a curved surface, considering the slip effects. The governing PDEs were transformed into nonlinear ODEs using the similarity transformation technique. The dimensionless system was then numerically solved using the BVP4C method in MATLAB. Various key parameters were systematically varied to analyze the behavior of velocity and temperature profiles. The following summarizes the main conclusions drawn from the current study:

- The velocity profile of the HNF improves with increasing volume fraction ϕ, suggesting that the use of HNFs could enhance the blood flow through narrowed arteries by improving fluid dynamics.
- Velocity decreases with higher values of porosity parameter, coefficient of inertia, curvature parameter, micropolar material parameter, unsteady parameter, and magnetic parameter. This indicates that the resistance to flow in a stenotic artery is influenced by these factors, affecting blood circulation in diseased or narrowed arteries.
- The temperature profile of the fluid increases with the porosity parameter, Eckert number, and unsteady parameter, highlighting the importance of efficient heat transfer for thermal regulation in blood flow through arteries.
- The HNF (blood–Au + TiO_2) demonstrates better heat transfer performance compared to the NF (blood–Au), especially with an increased porosity parameter. This suggests that the combination of TiO_2 and Au nanoparticles in HNFs can improve the thermal efficiency and offer potential for controlling temperature within arterial flow.
- The curvature parameter influences the micropolar profile with an increase in curvature leading to a decrease in micropolar behavior, which reflects how the narrowing and curvature of arteries affect fluid dynamics in the region of stenosis.
- Micropolar behavior is enhanced in HNFs (blood–Au + TiO_2), as compared to conventional NFs, under the influence of micro-inertia density and unsteady parameters. This behavior is critical in modeling blood flow in arteries where complex dynamics, such as micro-rotations and fluid deformations, are present.

The current study provides valuable insights into the flow dynamics of magnetized micropolar HNFS in stenotic arteries. However, several areas remain open for future exploration to further enhance our understanding and broaden the application of HNFs in medical contexts. While the current study employs numerical simulations, future research could focus on experimental studies to validate the numerical predictions of HNF behavior under real-world conditions. These experiments could focus on simulating arterial stenosis in laboratory settings and comparing results with computational models. Including biological factors such as red blood cell behavior, plasma blood viscosity, and the effects of pulsatile nature of blood flow could enhance the realism of the simulations and provide a more comprehensive understanding of blood flow dynamics in diseased arteries. By addressing these research directions, future studies could significantly contribute to the development of more effective medical treatments using HNFs for improving the blood flow, heat transfer, and overall vascular health.

Acknowledgments: This project was supported by the Ongoing Research Funding program, (ORF-2025-411), King Saud University, Riyadh, Saudi Arabia.

Funding information: This study was supported by the "Project financed by Lucian Blaga University of Sibiu through the research grant LBUS-IRG-2024."

Author contributions: All authors have accepted responsibility for the entire content of this manuscript and approved its submission.

Conflict of interest: The authors state no conflict of interest.

Data availability statement: The datasets generated and/or analyzed during the current study are available from the corresponding author on reasonable request.

References

[1] Xu H, Pop I. Mixed convection flow of a nanofluid over a stretching surface with uniform free streamin the presence of both nanoparticles and gyrotactic microorganisms. Int J Heat Mass Transf. 2014;75:610–23.

[2] Aziz A, Khan WA, Pop I. Free convection boundary layer flow past a horizontal flat plate embedded in porous medium filled by nanofluid containing gyrotactic microorganisms. Int J Therm Sci. 2012;56:48–57.
[3] Agarwal RS, Bhargava R, Balaji AVS. Finite element solution of flow and heat transfer of a micropolar fluid over a stretching sheet. Int J Eng Sci. 1989;27(11):1421–8.
[4] Hassanien IA, Gorla RSR. Heat transfer to a micropolar fluid from a non-isothermal stretching sheet with suction and blowing. Acta Mech. 1990;84(1–4):191–9.
[5] Rehman A, Khun MC, Khan D, Shah K, Abdeljawad T. Stability analysis of the shape factor effect of radiative on MHD couple stress hybrid nanofluid. South Afr J Chem Eng. 2023;46:394–403.
[6] Nadeem S, Rehman A, Vajravelu K, Lee J, Lee C. Axisymmetric stagnation flow of a micropolar nanofluid in a moving cylinder. Math Probl Eng. 2012;2012:1–18.
[7] Balaram M, Sastri VUK. Micropolar free convection flow. Int J Heat Mass Transf. 1973;16(2):437–41.
[8] Lok YY, Amin N, Pop I. Steady two-dimensional asymmetric stagnation point flow of a micropolar fluid. ZAMM - J Appl Math Mech/Z Angew Math Mech. 2003;83(9):594–602.
[9] Waini I, Ishak A, Pop I. Hybrid nanofluid flow and heat transfer past a vertical thin needle with prescribed surface heat flux. Int J Numer Methods Heat Fluid Flow. 2019;29(12):4875–94.
[10] Ashwinkumar GP, Samrat SP, Sandeep N. Convective heat transfer in MHD hybrid nanofluid flow over two different geometries. Int Commun Heat Mass Transf. 2021;127:105563.
[11] Samrat S, Ashwinkumar GP, Sandeep N. Simultaneous solutions for convective heat transfer in dusty-nano- and dusty-hybrid nanoliquids. Proc Inst Mech Eng E: J Process Mech Eng. 2021;236(2):473–9.
[12] Acharya N. Spectral quasi linearization simulation on the hydrothermal behavior of hybrid nanofluid spraying on an inclined spinning disk. Partial Differ Equ Appl Math. 2021;4:100094.
[13] Sarwar L, Hussain A. Flow characteristics of Au-blood nanofluid in stenotic artery. Int Commun Heat Mass Transf. 2021;127:105486.
[14] Garia R, Rawat SK, Kumar M, Yaseen M. Hybrid nanofluid flow over two different geometries with Cattaneo–Christov heat flux model and heat generation: A model with correlation coefficient and probable error. Chin J Phys. 2021;74:421–39.
[15] Eringen AC. Theory of micropolar fluids. J Math Mech. 1966;16(1):1–18.
[16] Shah Z, Sulaiman M, Dawar A, Alshehri MH, Vrinceanu N. Darcy–Forchheimer MHD rotationally symmetric micropolar hybrid-nanofluid flow with melting heat transfer over a radially stretchable porous rotating disk. J Therm Anal Calorim. 2024;149(24):14625–41. doi: 10.1007/s10973-024-12986-z.
[17] Deebani W, Shah Z, Rooman M, Khan NU, Vrinceanu N, Shutaywi M. Computational modelling of micropolar bloodbased magnetised hybrid nanofluid flow over a porous curved surface in the presence of artificial bacteria. Front Chem. 2024;12:1397066. doi: 10.3389/fchem.2024.139706.
[18] Hassanien IA, Gorla RSR. Heat transfers to a micropolar fluid from a non-isothermal stretching sheet with suction and blowing. Acta Mech. 1990;84(1–4):191–9.
[19] Subhani M, Nadeem S. Numerical analysis of micropolar hybrid nanofluid. Appl Nanosci. 2019;9(4):447–59.
[20] Hasegan A, Mihai I, Teodoru CA, Matacuta IB, Dura H, Todor SB, et al. Exploring the challenges of using minimal invasive surgery to treat stress urinary incontinence: insights from a retrospective case-control study. Diagnostics. 2024;14(3):323. doi: 10.3390/diagnostics14030323.
[21] Mihai I, Dura H, Teodoru CA, Todor SB, Ichim C, Grigore N, et al. Intraoperative ultrasound, bridging the gap between laparoscopy and surgical precision during 3D laparoscopic partial nephrectomies. Diagnostics. 2024;14:942. doi: 10.3390/diagnostics14090942.
[22] Mihai I, Boicean A, Teodoru CA, Grigore N, Iancu GM, Dura H, et al. Laparoscopic adrenalectomy: tailoring approaches for the optimal resection of adrenal tumors. Diagnostics. 2023;13(21):3351. doi: 10.3390/diagnostics13213351.
[23] Ghadikolaei SS, Yassari M, Sadeghi H, Hosseinzadeh K, Ganji DD. Investigation on thermophysical properties of Tio_2–Cu/H_2O hybrid nanofluid transport dependent on shape factor in MHD stagnation point flow. Powder Technol. 2017;322:428–38.
[24] Ullah I, Shafie S, Khan I. Effects of slip condition and Newtonian heating on MHD flow of Casson fluid over a nonlinearly stretching sheet saturated in a porous medium. J King Saud Univ - Sci. 2017;29(2):250–9.
[25] Gul A, Khan I, Shafie S, Khalid A, Khan A. Heat transfer in MHD mixed convection flow of a ferrofluid along a vertical channel. PLOS ONE. 2015;10(11):e0141213.
[26] Saqib M, Khan I, Shafie S. Natural convection channel flow of CMC-based CNTs nanofluid. Eur Phys J Plus. 2018;133(12):549.
[27] Ma Y, Mohebbi R, Rashidi MM, Yang Z, Sheremet MA. Numerical study of MHD nanofluid natural convection in a baffled U-shaped enclosure. Int J Heat Mass Transf. 2019;130:123–34.
[28] Khan LA, Raza M, Mir NA, Ellahi R. Effects of different shapes of nanoparticles on peristaltic flow of MHD nanofluids filled in an asymmetric channel: A novel mode for heat transfer enhancement. J Therm Anal Calorim. 2020;140(3):879–90.
[29] Ghalambaz M, Mehryan SAM, Izadpanahi E, Chamkha AJ, Wen D. MHD natural convection of Cu–Al_2O_3 water hybrid nanofluids in a cavity equally divided into two parts by a vertical flexible partition membrane. J Therm Anal Calorim. 2019;138(2):1723–43.
[30] Zeb S, Gul S, Shah K, Santina D, Mlaiki N. Melting heat transfer and thermal radiation effects MHD tangent hyperbolic nanofluid flow with chemical reaction and activation energy. Therm Sci. 2023;27(Spec. issue 1):253–61.
[31] Das S, Jana RN, Makinde OD. MHD flow of Cu-Al_2O_3/water hybrid nanofluid in porous channel: Analysis of entropy generation. Defect Diffus Forum. 2017;377:42–61.
[32] Anantha Kumar K, Sugunamma V, Sandeep N. Influence of viscous dissipation on MHD flow of micropolar fluid over a slendering stretching surface with modified heat flux model. J Therm Anal Calorim. 2020;139(6):3661–74.
[33] Khan A, Ullah S, Shah K, Alqudah MA, Abdeljawad T, Ghani F. Theory and semi-analytical study of micropolar fluid dynamics through a porous channel. CMES-Comput Model Eng Sci. 2023;136(2):1473–86.
[34] Boicean A, Bratu D, Bacila C, Tanasescu C, Fleaca RS, Mohor CI, et al. Therapeutic perspectives for microbiota transplantation in digestive diseases and neoplasia – A literature review. Pathogens. 2023;12(6):766.
[35] Pirvut V, Grigore N, Mihai I, Priporeanu AT, Racheru M, Cretu D, et al. Comparative study between polydioxanone unidirectional barbed suture and absorbable polyglactin running suture in partial nephrectomy. Rev Mater Plast. 2018;54:82–4.
[36] Dawar A, Shah Z, Kumam P, Alrabaiah H, Khan W, Islam S, et al. Chemically reactive MHD micropolar nanofluid flow with velocity slips and variable heat source/sink. Sci Rep. 2020;10(1):20926.

[37] Sakiadis BC. Boundary-layer behavior on continuous solid surfaces: I. Boundary-layer equations for two-dimensional and axisymmetric flow. AIChE J. 1961;7(1):26–8.
[38] Tsou FK, Sparrow EM, Goldstein RJ. Flow and heat transfer in the boundary layer on a continuous moving surface. Int J Heat Mass Transf. 1967;10(2):219–35.
[39] Crane LJ. Flow past a stretching plate. ZAMP Z Angew Math Phys. 1970;21(4):645–7.
[40] Gupta PS, Gupta AS. Heat and mass transfer on a stretching sheet with suction or blowing. Can J Chem Eng. 1977;55(6):744–6.
[41] Grubka LJ, Bobba KM. Heat transfer characteristics of a continuous, stretching surface with variable temperature. J Heat Transf. 1985;107(1):248–50.
[42] Das S, Pal TK, Jana RN, Giri B. Significance of Hall currents on hybrid nano-blood flow through an inclined artery having mild stenosis: homotopy perturbation approach. Microvasc Res. 2021;137:104192.
[43] Karmakar P, Ali A, Das S. Circulation of blood loaded with trihybrid nanoparticles via electro-osmotic pumping in an eccentric endoscopic arterial canal. Int Commun Heat Mass Transf. 2023;141:106593.
[44] Ali A, Das S. Applications of neuro-computing and fractional calculus to blood streaming conveying modified trihybrid nanoparticles with interfacial nanolayer aspect inside a diseased ciliated artery under electroosmotic and Lorentz forces. Int Commun Heat Mass Transf. 2024;152:107313.
[45] Paul P, Karmakar P, Das S, Das S. Demonstration of angioplasty using a balloon catheter in tetra-hybrid nano-bloodstream within an electrified stenotic arterial cavity under a magnetic field: Artificial neural network analysis. Biomed Signal Process Control. 2024;96:106549.
[46] Haq F, Shah K, Abdeljawad T. Analysis of periodic heat transfer through extended surfaces. Therm Sci. 2023;27(4 Part A):2623–37.
[47] Ahmad L, Khan M. Importance of activation energy in development of chemical covalent bonding in flow of Sisko magneto-nanofluids over a porous moving curved surface. Int J Hydrogen Energy. 2019;44(21):10197–206.
[48] Sheikholeslami M, Arabkoohsar A, Babazadeh H. Modeling of nanomaterial treatment through a porous space including magnetic forces. J Therm Anal Calorim. 2020;140(2):825–34.